Luminescent gold(I) complexes of 1-pyridyl-3-anthracenyl-chalcone inducing apoptosis in colon carcinoma cells and antivascular effects.

Juan Jesús González,[1] Enrique Ortega,[1] Matthias Rothemund,[2] Madeleine Gold,[2] Consuelo Vicente,[1] Concepción de Haro,[1] Delia Bautista,[3] Rainer Schobert,[2,*] José Ruiz[1,*]

[1]Departamento de Química Inorgánica, Facultad de Química, Biomedical Research Institute of Murcia (IMIB-Arrixaca-UMU), Universidad de Murcia, E-30071 Murcia, Spain; Tel: + 34 868887455. E-mail: jruiz@um.es

[2]Organic Chemistry Laboratory, University Bayreuth Universitaetsstrasse 30, 95440 Bayreuth (Germany). E-mail: rainer.schobert@uni-bayreuth.de

[3]SAI, Universidad de Murcia, E-30071 Murcia, Spain.

Abstract

The luminescent chalcone gold(I) conjugates $[Au(PPh_3)(AN3E)]PF_6$ (**1**) and $[Au(SIMes)(AN3E)]PF_6$ (**2**) (AN3*E* = (*E*)-3-(9-anthracenyl)-1-(4-pyridyl)propenone; SIMes = N,N′-dimesitylimidazolidin-2-ylidene; Mes = 2,4,6-trimethylphenyl)) were prepared and characterized, complex (**1**) also characterized by X-ray crystallography. In MTT assays against a panel of three human colon, a melanoma and a breast cancer cell lines both complexes were antiproliferative with low micromolar IC_{50} values. Noteworthy, $HCT116^{p53-/-}$ colon carcinoma cells lacking functional p53 (a vital tumor suppressor) were more susceptible to them than the wildtype parent cell line. In flow cytometry analyses the gold conjugates induced a significant arrest in G_2/M phase primarily. Complexes **1** and **2** quickly increased the production of reactive oxygen species (ROS) and induced mitochondrial membrane potential depolarization, higher ROS values being obtained after co-administration with enzymatic inhibitors. The free chalcone AN3*E* and its gold(I) complex conjugates located in the cell mitochondria according to confocal microscopy. In addition, complexes **1** and **2** showed *in vivo* antivascular effects on the chorioallantoic membrane (CAM) of fertilized specific-pathogen-free (SPF) chicken eggs.

INTRODUCTION

Gold(I) complexes have recently emerged as a potential chemotherapeutic alternative to conventional medical cancer treatments based on platinum(II) agents, such as Cisplatin (CDDP) or Oxaliplatin (OXP).[1,2] Wiping out side-effects and improving biological activity have become the main purposes of new antitumor compounds research, which eventually led to the development of several innovative therapeutic strategies. In fact, numerous gold complexes with antitumor activity have been previously reported,[3-10] and even the established antiarthritic gold(I) thiolate drug Auranofin is currently undergoing evaluation in different US clinical trials because of its antineoplastic properties.[11]

In the current context, *N*-heterocyclic carbene (NHC) gold-derivatives have garnered greater and greater attention as anticancer agents, lately, because of their stability under physiological conditions and biological activity,[12-18] mainly due to their excellent sigma-donating capacity and easy modulation of both the steric and electronic properties. Moreover, gold(I) phosphine complexes display remarkable anticancer properties since their lipophilicity facilitates transport across cell membranes.[19-21]

On the other hand, keeping in mind that half of current treatments in human neoplasms therapy are dependent on functional p53-protein, the use of chalcones as auxiliary ligands is a particularly promising aspect in the design of novel anti-cancer agents Evidence is growing that chalcones are effective inhibitors of the p53-MDM2 interaction, as, for instance, recently reported for the platinum(IV) derivative prodrugs chalcoplatin and monochalcoplatin.[22,23] Chalcoplatin arrests the cell cycle at G2/M phase, significantly induces p53 activation and triggers downstream apoptotic pathways, which is a mechanism of action that indicates the role of the p53 agonist. The p53-dependent anticancer activity of the Au(I) NHC complex MC3 has been recently reported,[24] whereas Auranofin acts as an apoptosis inducer in tumor cells by means of an oxidative stress pathway not p53-dependent.[25]

We report herein the synthesis of two novel luminescent chalcone gold(I) conjugates containing the 9-anthracenyl substituted pyridyl enone AN3*E*, a fragment with interesting pharmacological properties,[26-28] even when it acts as a coordination ligand.[29] The anticancer activity of the new complex conjugates has been evaluated against a panel of six human cancer cell lines of three different entities with a mechanistic focus on colon carcinoma cells.

RESULTS AND DISCUSSION

Synthesis of the New Gold(I) Complexes.

The gold(I) conjugates $[Au(PPh_3)(AN3E)]PF_6$ (**1**) and $[Au(SIMes)(AN3E)]PF_6$ (**2**) were obtained (Scheme 1) in high yields (77 and 92%, respectively) from the reaction of the chalcone ligand AN3*E* in the proper molar ratio and solvent with $[AuCl(PPh_3)]$ or $[AuCl(SIMes)]$, respectively, in the presence of $AgNO_3$ and NH_4PF_6.
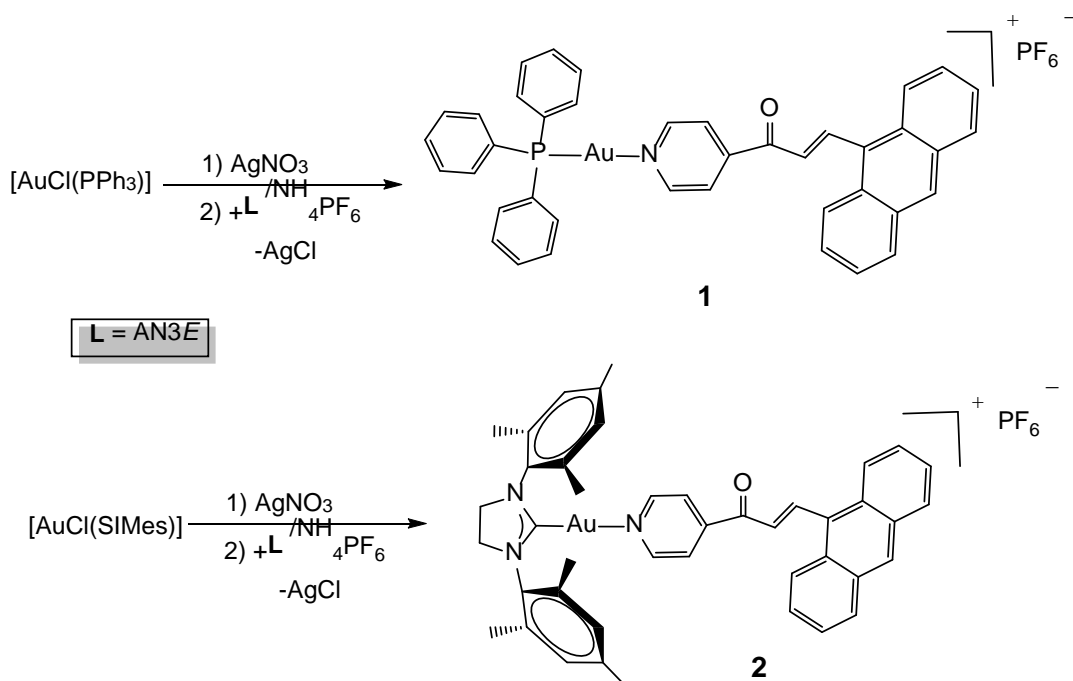
Scheme 1. Synthetic routes for complexes **1** and **2**.

Complexes were characterized by NMR spectroscopy in CDCl$_3$ (Fig. S2 − S13[†]). The coupling constant of J_{H-H} = 16 Hz observed in both complexes' spectra caused by olefin protons resonance confirms the *E*-configuration of the chalcone ligand. Elemental analysis showed a purity of at least 95% for these complexes, and their positive ion ESI-MS displayed the [M]$^+$ peaks in agreement with the calculated isotopic pattern (Fig. S14[†]).

Photophysical properties

Both complexes were characterized also by UV-vis spectroscopy and fluorescence spectroscopy in DMSO solution (Fig. S18-20[†]). Absorption (λ_{abs}), excitation (λ_{exc}) and emission (λ_{em}) wavelengths, emission lifetimes (τ_{em}) and quantum yields (Φ_{em}) data for gold compounds and AN3*E* ligand in two different solvents have been tabulated (Table 1).

Table 1 Photophysical properties of the compounds in different solvents.

| Compound	λ_{abs}, nm[a] (ε, M$^{-1}\cdot$cm^{-1})	λ_{exc}, nm	λ_{em}, nm	τ_{em}, ns[b] (%)	Φ_{em},%[c]
(1)	258 (92881), 426 (7720)	492[a]	571[a]	-	-
	-	385[b]	449[b]	479 (91.6) 54 (8.4)	< 1.0
(2)	259 (93240), 426 (6860)	492[a]	571[a]	-	-
	-	387[b]	478[b] 451[b] 422[b]	147 (80.6) 8 (19.4)	1.2
AN3E	259 (12975), 423 (1282)	506[a]	568[a]	-	-
	-	420[b]	514[b]	105 (100)	1.4

[a] In DMSO solution. [b,c] In aerated and deaerated PBS/DMSO (99:1) medium, respectively.

The electronic absorption spectra obtained for complexes **1** and **2** in DMSO solution showed two defined intraligand (IL) transitions brought about by the chalcone group.[30] Their emission spectra in this solvent featured maxima around 570 nm, giving Stokes shifts of 62–79 nm, so that the luminescent properties of the complexes in DMSO could be attributed to the chalcone moiety.

The compounds were also studied in phosphate buffered saline (PBS) with 1% of DMSO. An emission maximum was observed for AN3*E* (Fig. S22[†]) and for **1** (Fig. S23[†]) at 514 nm and 449 nm, respectively, while a structured emission band was found for **2**, with an emission maximum at 478 nm, presumably due to the carbene ligand (Fig. S24[†]).

The emission lifetimes of the compounds were measured in PBS/DMSO (99:1) and the double exponential decays observed for the gold(I) complexes suggested the simultaneous existence of two excited states, whose pertinent contributions to the luminescent properties are shown in brackets in Table 1. Low quantum yields were registered in this latter medium.

X-ray Crystal Structure of Complex 1. Single crystals of (C$_{40}$H$_{30}$AuNOP)·(PF$_6$)·0.5CH$_2$Cl$_2$ suitable for X-ray diffraction analysis were obtained from dichloromethane/hexane. Crystallographic data are given in Tables S1–S3. The gold atom (Fig. 1) is coordinated to the phosphorus atom and the N-atom of the pyridyl chalcone in an approximately linear manner. The Au–P bond distance is similar to those found in other gold(I) phosphine complexes.[31] Intermolecular π–π interactions between chalcone ligands are observed (Fig. S26[†]).[32] No aurophilic bonds between the two gold(I) centers are observed (Au···Au distances > 6.85 Å).
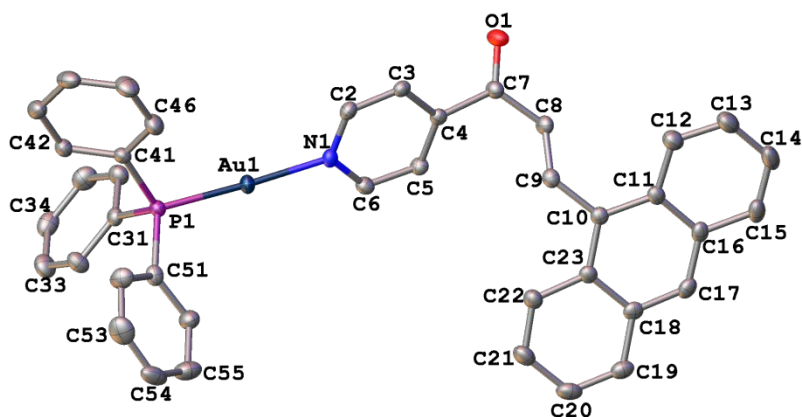
Fig. 1 X-ray crystal structure of the cation of gold complex **1** with atom numbering scheme (50% thermal ellipsoids). Selected bond lengths (Å) and angles (deg): Au(1)–P(1) = 2.2314(12), Au(1)–N(1) = 2.0723(17), P(1)–Au(1)–N(1) = 177.10(4).

Stability studies

The stability of the gold(I) compounds has been tested in different media (DMSO and DMSO/H_2O/Cl$^-$, [NaCl] = 100 mM) by ESI$^+$ (Fig. S27-S30†) and it was also confirmed in the solvent mixture DMSO/DMEM (Dulbecco's Modified Eagle Medium) by absorption spectroscopy. The complexes remained unaltered even after 72 h in solution at RT in every case (Fig. S31†).

Cytotoxicity

The anticancer activities of the prepared gold(I) complexes were evaluated in a panel of human colon, melanoma and breast cancer cells as well as in one non-malignant human dermal fibroblast cell line (HDFa) by means of MTT-based proliferation assays. Cisplatin was also evaluated under the same experimental conditions. The IC_{50} values obtained shown in Table 2 range from 1 to 7 µM against the tested cell lines. Noteworthy, both complexes exhibited a higher cytotoxic effect against p53-deficient HCT-116 colon cancer cells compared to the wild type HCT-116^{wt} cells, which suggested a p53-dependence in their mechanism of action. In contrast, the free chalcone ligand AN3*E* was three times less active than the new gold conjugates in HCT-116$^{p53-/-}$ cancer cells. Against the non-malignant HDFa fibroblasts the complexes **1** and **2** were two to three times less cytotoxic when compared with the malignant cell lines.

Table 2 Means ± SD of IC$_{50}$[a] (72 h) values [μM] of complexes **1**, **2** and cisplatin in MTT assays against human HT29, HCT116^{wt} its p53 knock out mutant HCT116$^{p53-/-}$, DLD-1 colon carcinoma, 518A2 melanoma and MCF-7^{Topo} breast carcinoma, as well as the non-malignant HDFa dermal fibroblasts.

	HT29	HCT-116^{wt}	HCT-116^{-p53}	DLD-1	518A2	MCF-7^{Topo}	HDFa
1	2.1 ± 0.1	6.8 ± 0.5	3.6 ± 0.1	3.8 ± 0.1	4.7 ± 0.2	4.1 ± 0.3	7.2 ± 1.6
2	6.2 ± 0.1	6.7 ± 0.3	4.0 ± 0.1	3.6 ± 0.01	1.1 ± 0.1	7.0 ± 1.0	11.4 ± 1.9
AN3*E*	7.3 ± 1.2	15.9 ± 3.1	12.8 ± 1.7	8.6 ± 0.3	8.1 ± 0.4	11.0 ± 0.9	
Cisplatin	6.2 ± 1.1	5.7 ± 0.3[b]	9.2 ± 0.5[b]	5.5 ± 0.2[b]	2.6 ± 0.7[b]	13.5 ± 1.7[b]	

[a] Values are derived from dose–response curves obtained by measuring the percentage of vital cells of treated wells relative to untreated controls after 72 h of incubation using MTT-assays. Values are means ± SD of four independent experiments.
[b]Source of Cisplatin IC$_{50}$ Values.[33]

## Cellular uptake and accumulation in cancer cells.

The new gold complexes accumulate effectively within HT29 colon carcinoma cells after 24 h drug-exposure as determined by measuring the amount of Au by ICP-MS. Both gold complexes accumulated to a greater extent than Cisplatin in these cells, and complex **1** led to a much higher intracellular metal concentration than complex **2** (Table 3).

Table 3 Cellular gold and platinum accumulation in HT29 cancer cells after 24 h treatment with 10 μM of either **1, 2** or Cisplatin. Measurements indicate total cellular uptake of ^{197}Au for tested compounds and ^{195}Pt for Cisplatin. Negative references for ^{197}Au and ^{195}Pt from untreated cells are denoted by "[a]" and "[b]", respectively.

	ng/10^6 cells
Untreated cells[a]	0.12 ± 0.05
Untreated cells[b]	0.09 ± 0.04
1	266.31 ± 6.82
2	55.70 ± 2.54
Cisplatin	12.06 ± 1.54

Due to the intrinsic fluorescence of the ligand and the complexes, their localization within HT29 cancer cells was investigated by confocal microscopy (Fig. 2). Mitochondria were stained for 30 min with 150 nM of the far-red-fluorescent dye MitoTracker Red. After 4 h of incubation with **1**, **2** or ligand AN3*E* (20 μM), the

chalcone compounds were excited at a wavelength that does not interfere with the MitoTracker Red dye. The fluorescence of **1**, **2** and AN3*E* was well visible in the cancer cells. It could be superimposed with the fluorescence by MitoTracker Red dye without any offset (Fig. 2).

	Bright Field	λ=645 nm (MT Deep Red)	λ=405 nm	Overlay
Control				
1				
2				
AN3*E*				
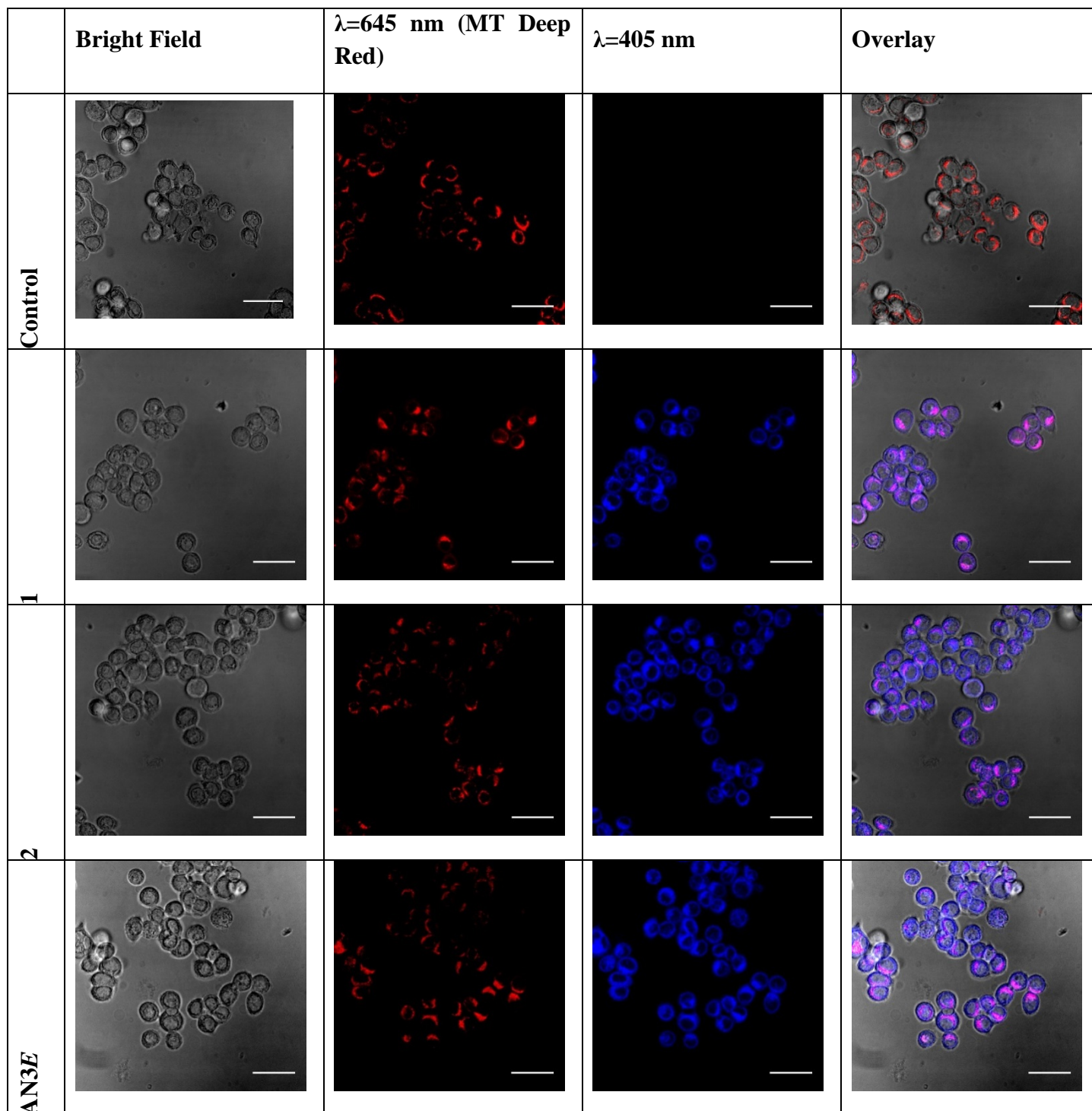
Fig. 2 Confocal microscopy images of HT29 cells treated with 20 µM of gold complexes **1**, **2** or ligand AN3*E* for 4h and stained with MitoTracker Deep Red (150 nM) for 30 min. Scale bar = 40 µm.

Mitochondrial polarization assay

Since any depolarization the mitochondrial membrane potential (MMP) of cells can trigger apoptotic cell death, the impact of the gold complexes **1** and **2** on the mitochondrial membrane potential of HT29 cells was evaluated using the dye Rhodamine-123.[34] Treatment with 10 µM of **1** and **2** caused a loss in Rhodamine-123 fluorescence intensity after 24 h, indicating a depolarization of the MMP (Fig. 3).
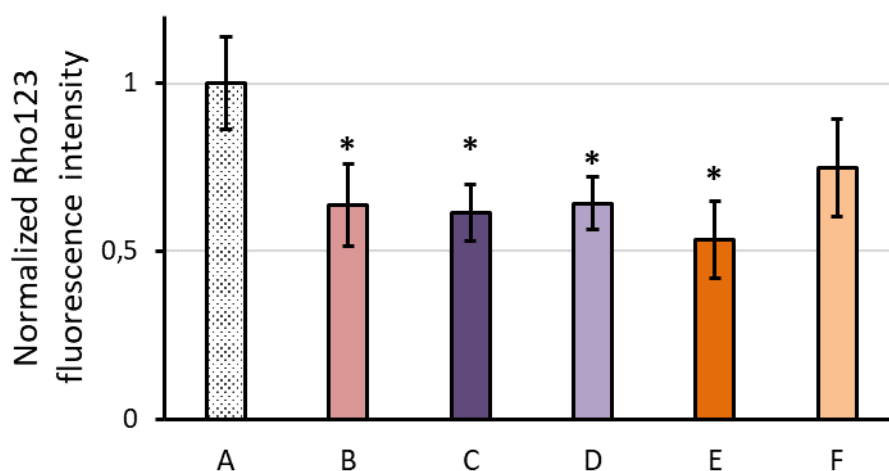

Fig. 3 Effect of Au complexes **1** and **2** on the mitochondrial membrane potential of HT29 colon carcinoma cells measured by Rhodamine 123 (Rho123) fluorescence intensity. Untreated cells were used as a negative control whereas carbonyl cyanide m-chlorophenyl hydrazone (CCCP, 10 µM) treatment was used as a positive control for mitochondrial membrane depolarization. A) Untreated control, B) [CCCP] = 10 µM, C) [**1**] = 20 µM, D) [**1**] = 10 µM E) [**2**] = 20 µM, F) [**2**] = 10 µM. Results are presented as mean ± SD, *p < 0.05 (unpaired t-test).

Apoptosis induction

The induction of apoptosis in HT29 cells exposed to **1** and **2** was investigated by flow cytometry using Annexin-V/PI dual-staining, which allowed the differentiation of four cell populations: live cells, necrotic cells and early/late apoptotic cells. Early apoptosis, which is characterized by changes in the symmetry of the phospholipid membrane, is represented in the Annexin V^+/PI$^-$ quadrant whereas late apoptotic stage, where further membrane disruption allows PI entering the cells is depicted in the Annexin V^+/PI$^+$ quadrant. Both complexes **1** and **2** when applied at 10 µM increased the cell populations in early and late apoptosis after 24 hours, revealing a similar dot plot profile as

cisplatin-treated cells (Fig. 4). These results indicated that the cell death induced by the new gold complexes is mainly due to apoptosis rather than necrosis.
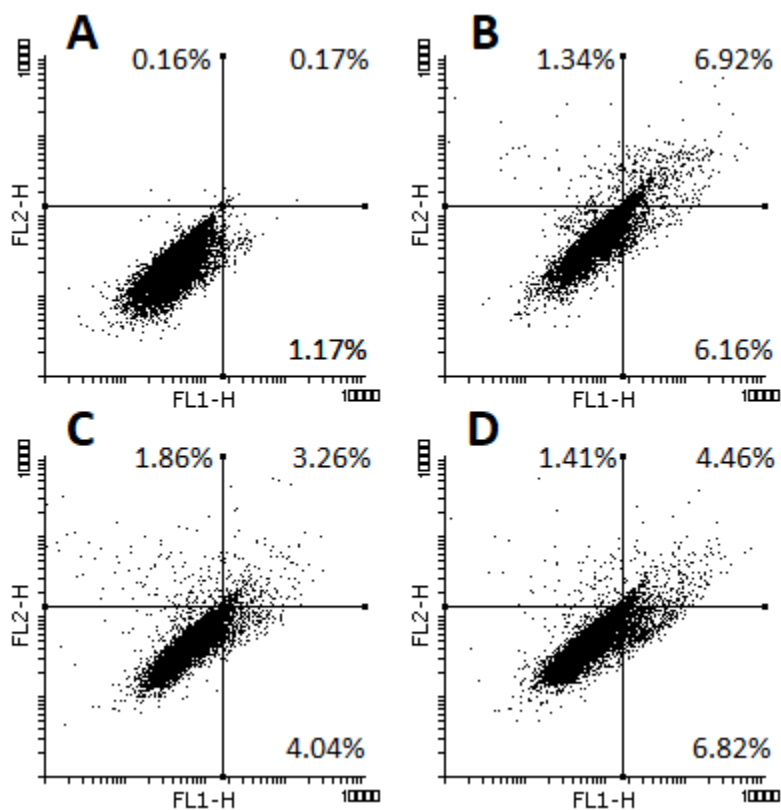
Fig. 4 Representative dot plots obtained by flow cytometric analysis of HT29 cells left untreated (A) or treated for 24 h with either Cisplatin (B) or Au compounds **1** (C) and **2** (D) at 10 µM, detected by Annexin V-FITC (FL1-H)/propidium iodide (FL2-H) dual staining method.

Generation of ROS

Cancer cells usually have increased levels of reactive oxygen species (ROS) compared to normal cells. However, excessive amounts of ROS lead to oxidative damage to essential macromolecules such as DNA or proteins. Following a treatment (2 h) with complexes **1** and **2**, the intracellular ROS levels of HT29 cells were measured using the 2'7'-dichlorodihydrofluorescein diacetate (DCFH-DA) probe. DCFH-DA is rapidly cleaved by intracellular esterases into its form DCFH which is converted to the fluorescent product 2',7'-dichlorofluorescein (DCF) in the presence of ROS.[35] As shown in Fig. 5, both complexes induced a significant generation of ROS after 2 h compared to untreated cells, indicating that the compounds could act as potent oxidants within the cell. No changes in ROS levels were observed upon treatment with the free ligand AN3*E*. In addition, co-treatment with the well-known ROS scavenger N-acetyl-L-cysteine (NAC) reversed the intracellular ROS levels induced by the gold complexes.
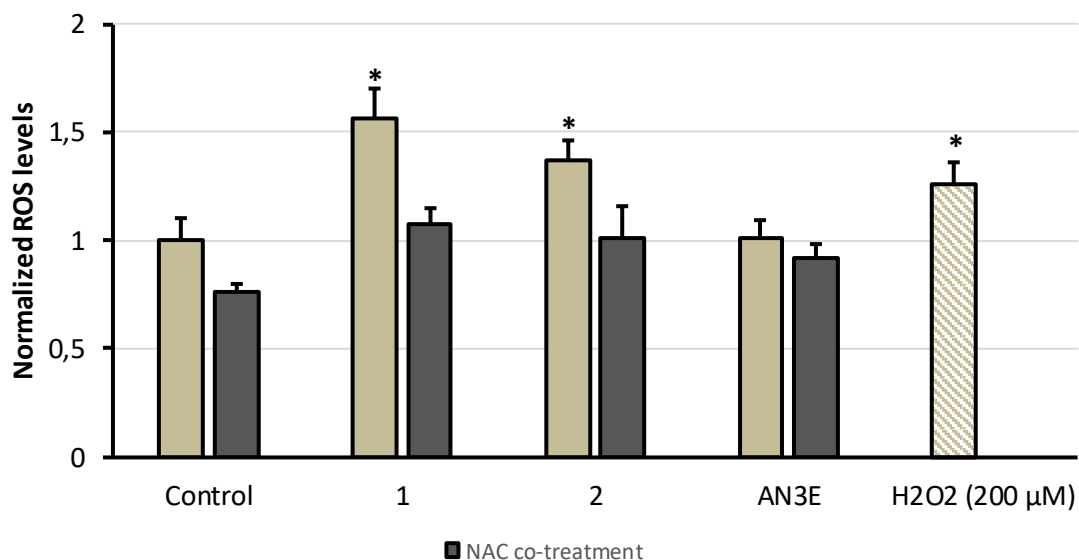
Fig. 5. ROS induction in HT29 cells upon 2 h treatment with 10 µM of complexes **1** or **2** or ligand AN3*E,* or co-treatment with 2 mM N-acetyl-cysteine (NAC), measured using DCFH-DA (10 µM). Untreated cells served as negative control whereas hydrogen peroxide (H_2O_2) was used as a positive control for ROS induction. Statistical data are shown as mean ± SD *p<0.05 (n = 4).

Glutathione (GSH) and the antioxidant enzyme catalase play important roles as scavengers of ROS. L-Buthionine-sulfoximine (L-BSO) can be used to deplete intracellular levels of GSH through γ-glutamylcysteine synthetase inhibition whereas 3-amino-1,2,4-triazole (AMT) can lead to catalase inhibition (Fig. 6). This suggests that the complexes rapidly induce ROS formation and co-administration of complexes with non-toxic doses of L-BSO or AMT potentiates a synergistic rise of ROS levels in cancer cells, which may be related to mitochondrial dysfunction.
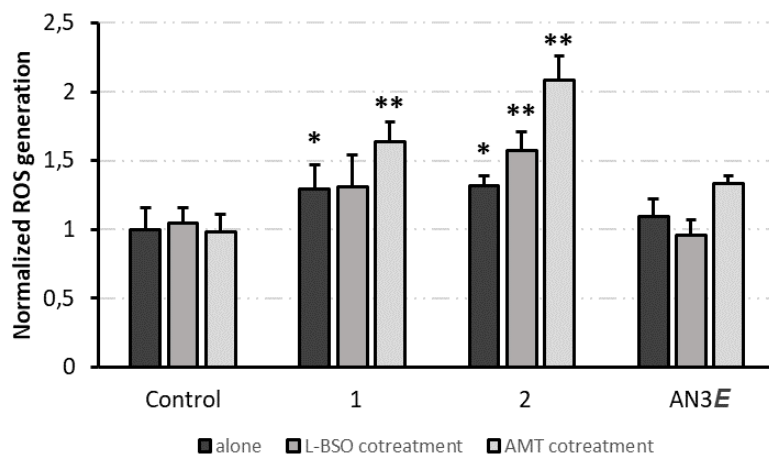
Fig. 6. Measurements of ROS in HT29 cells upon 2 h treatment with 10 µM of complexes **1** or **2** or ligand AN3*E* or cotreatment with L-BSO (500 µM) or AMT (500 µM) using DCFH-DA (10 µM). Statistical data are shown as mean ± SD *p<0.05 and **p<0.01 (n=4).

Cell cycle distribution perturbance by Au(I) compounds 1 and 2

To further characterize the mechanism of action of the new complexes, HT29 cells treated with tested compounds or cisplatin for 24 h were analyzed by flow cytometry using propidium iodide staining. Cell cycle profiles of HT29 treated cells showed increased percentage of cells in G_2/M phase with a concomitant reduction in G_0/G_1 population (Fig. 7). This dysregulation of cell cycle distribution could be related to the drug-induced insults of ROS, which might ultimately produce DNA damage and G_2/M arrest. The cell cycle distribution perturbance by the free ligand AN3*E* was completely different.


11
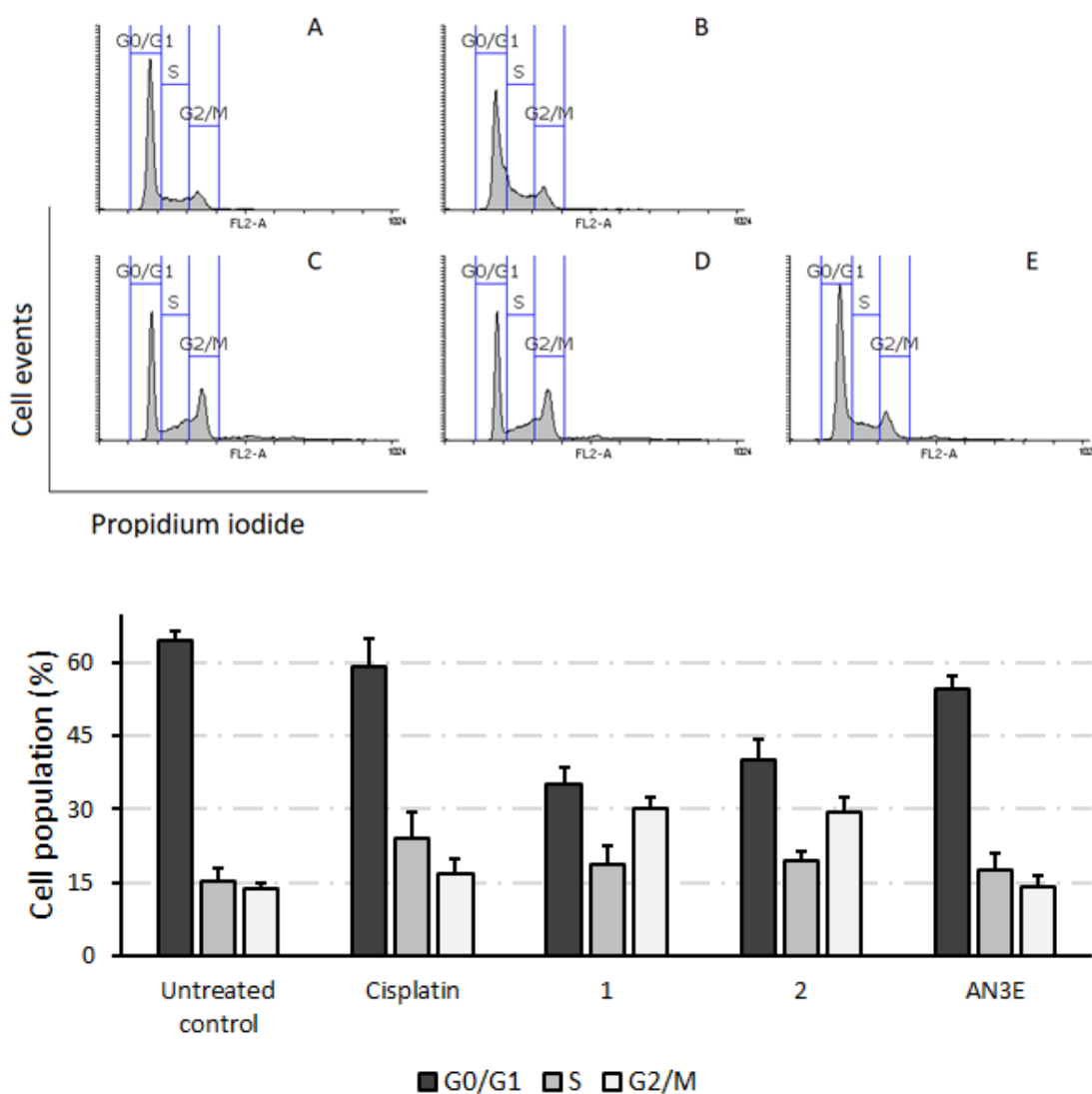
Fig. 7. Cell cycle analysis of HT29 cells treated with 10 µM gold complexes, ligand or cisplatin for 24 h using propidium iodide staining. (A) Untreated Control, (B) Cisplatin, (C) **1**, (D) **2**, (E) AN3*E*.

***In vitro* interaction studies with DNA.** Mitochondrial DNA (mtDNA) has recently emerged as a potential target for cancer therapy because of its greater vulnerability to pharmacological agents in relation to nuclear DNA, which could help overcome resistance to current antitumoral metal complexes.[36] As mitochondria seem to be a biological target of the new chalcone gold(I) complex conjugates, various interaction studies have been undertaken.

Reaction with 9-Ethylguanine (9-EtG). The interaction between the gold(I) conjugates **1** and **2** and 9-EtG was studied by ESI-MS (positive mode). Mass spectra (Fig. S32-S33[†]) showed peaks corresponding to the AN3*E* ligand displacement and the subsequent 9-EtG coordination to the gold center, even after 24 h of reaction, what suggests that covalent binding is favored.

Competition Binding Experiment with Calf Thymus DNA. Hoechst 33258 binds to the minor groove of DNA, increasing significantly its fluorescence yield. When the complexes were added to DNA-Hoechst solution, a decrease in the emission maximum of the dye was observed, due to the displacement of bound Hoechst 33258 from its binding site on ct-DNA. The difference between the effects of complexes **1** and **2** suggests that **2** binds more strongly to the minor groove of DNA than **1** (Fig. 8).
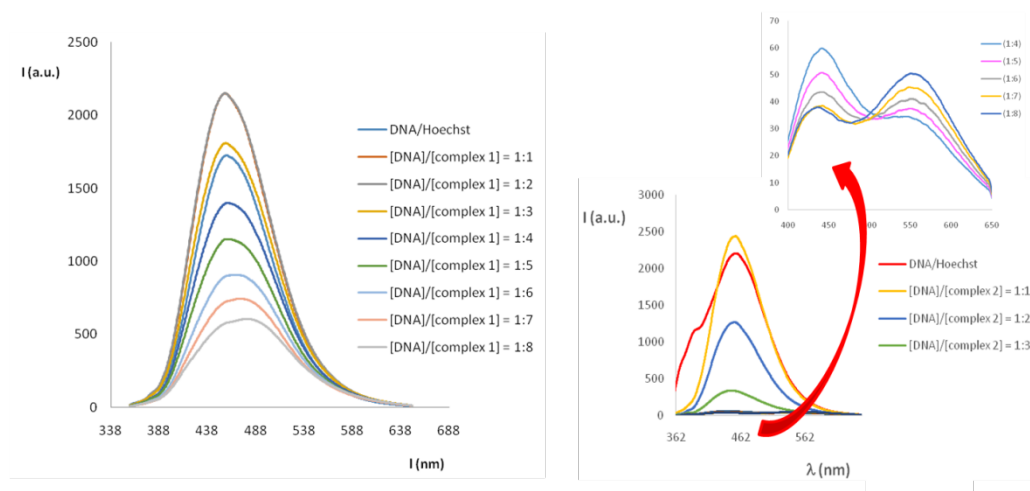
Fig. 8. Emission spectra of Hoechst 33258 bound to ct-DNA in absence and presence of increasing amounts of complexes **1** (left) and **2** (right). [Hoechst] = 2 µM, [ct-DNA] = 20 µM, [complexes] ~ 0-160 µM, pH = 7 y T = 298 K.

EtBr-saturation assays. Competitive binding experiments were also carried out to explain further the interactions of the new Au(I) complexes with DNA using an ethidium bromide displacement assay which is based on the replacement of ethidium bromide (EtBr) already bound to DNA with a test compound that also interacts with DNA. Fluorescence of EtBr was monitored (λ_{ex} = 535 nm, λ_{em} = 595 nm) at a fixed

concentration of salmon sperm DNA pretreated with EtBr during titration with increasing concentrations of **1** and **2**. As shown in Fig. 9 compound **1** exhibited a medium to good affinity for DNA, whereas complex **2** showed only a weak effect.
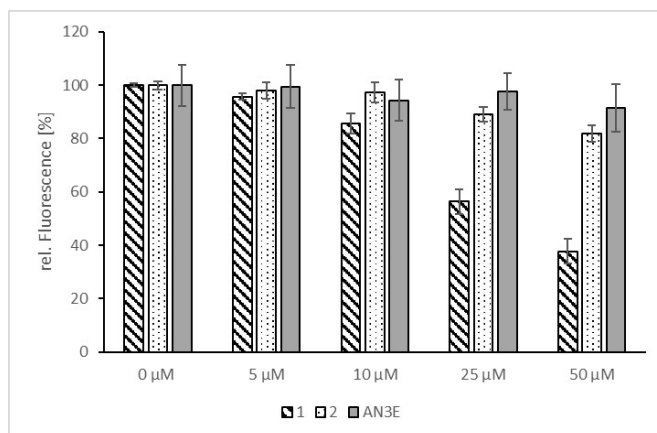

Fig. 9. Relative fluorescence intensities of EtBr bound to salmon sperm DNA in the presence of gold complexes and AN3*E* in TE buffer (10 mM Tris/HCl, 1 mM EDTA, pH 8.0). Error bars representing SD are smaller than symbols.

Electrophoretic mobility shift assay (EMSA) with pBR322 plasmid DNA. Because of the interaction between the gold(I) conjugates with 9-EtG observed by ESI-MS (see above), the DNA binding of complexes **1** and **2** was studied also by reacting them with pBR322 plasmid DNA at 37 °C for 24 h and separating the products using gel electrophoresis.[37] However, there was no effect visible in EMSA for the compounds (Fig. S34).

Antivascular activity. The *in vivo* antivascular effects of **1** and **2** was studied by using the CAM assay with fertilized SPF chicken eggs as a model system.[38] Fig. 10 shows the effect of 6 h treatment of the vascularized chorioallantoic membrane with **1** and **2** at 15 nmol in comparison with the control, treated with equivalent amounts of DMSO. Both compounds showed disrupting effects on the blood vessels in the CAM, with the small capillaries disappearing and bigger vessels getting eroded.
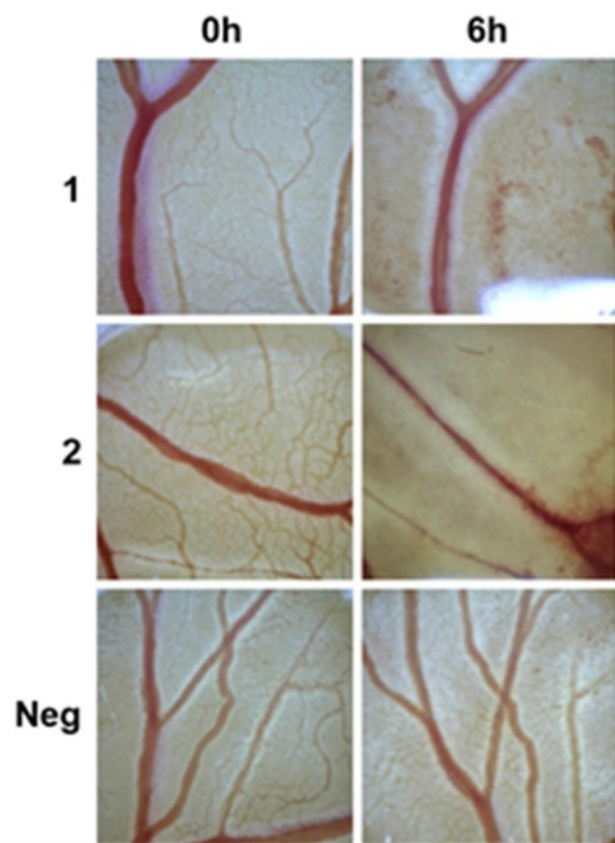
Fig. 10. Effects on the CAM of fertilized SPF chicken eggs upon treatment with 15 nmol of **1** and **2** for 6 h. The negative control contained an equal amount of DMSO; images are representative of three independent experiments. Magnification 60×.

Conclusions

The two novel targeting mitochondria chalcone gold(I) luminescent complexes of the type [Au(L)(AN3E)]PF$_6$ (L = PPh$_3$ **1**, SIMes **2**) exhibited selectivity against cells HCT116$^{p53-/-}$ colon carcinoma cells lacking functional p53 compared to its wild-type lineage. They quickly increased the production of ROS in HT29 cells and showed disrupting effects on the blood vessels in the CAM of fertilized SPF-eggs. Taken together, **1** and **2** showed the potential applications of theranostic gold(I) conjugates for treatment of cancers in which the p53 gene is lacking, and for some other CDDP-resistant cancers.

Acknowledgments

EXPERIMENTAL SECTION

Instrumental Measurements. The C, H and N analyses were performed with a Carlo Erba model EA 1108 microanalyzer. Decomposition temperatures were determined with

a SDT 2960 simultaneous DSC-TGA from TA Instruments at a heating rate of 5 ºC min^{-1} and the solid samples under nitrogen flow (100 mL min^{-1}). The ^{1}H, ^{13}C and ^{31}P NMR spectra were recorded using deuterated chloroform as a solvent on a Bruker AV 400 spectrometer, with tetramethylsilane (TMS) as internal standard for the ^{1}H and ^{13}C spectra and 85% H_3PO_4 for the ^{31}P spectra. ESI mass (positive mode) analyses were performed on a HPLC/MS TOF 6220. UV/vis spectroscopy was carried out at 10^{-4} M of complexes in DMSO on a Perkin-Elmer Lambda 750 S spectrometer with operating software. Fluorescence measurements were carried out at 10^{-5} M of complexes in DMSO and in PBS/DMSO (99:1) with a Perkin-Elmer LS 55 50 Hz Fluorescence Spectrometer. Excited-states lifetimes were measured using a NanoLED (λ_{exc} =372 nm).

Starting Materials and Reagents. All synthetic manipulations were carried out under a protective atmosphere of nitrogen using standard Schlenk techniques and solvents were dried by the usual methods. The starting complex [AuCl(tht)] (tht = tetrahydrothiophene) was prepared by a procedure described elsewhere.[39] The compound [AuCl(PPh$_3$)] was synthesized by reacting [AuCl(tht)] with PPh$_3$ in a 1:1 molar ratio in chloroform, likewise the starting complex [AuCl(SIMes)] was prepared by transmetalation of [AuCl(tht)] with the silver carbene [AgCl(SIMes)] in a stoichemistry ratio in dichloromethane.[40] [AgCl(SIMes)] was prepared by Ag$_2$O and SIMes·HCl reaction in the proper molar ratio. AN3*E* was synthesized by using procedures adapted from the literature.[41] Hoechst-33258, ethidium bromide, SIMes·HCl, PPh$_3$, 9-antraldehyde, tht and 4-acetylpyridine were obtained from Sigma-Aldrich (Madrid, Spain); tetrachloroauric acid trihydrate from Johnson Matthey (Royston, United Kingdom); deuterated solvents from Euriso-top and Tris-HCl buffer and sodium salt of calf thymus DNA (ct-DNA) and salmon sperm DNA from Eurofins.

Synthesis and characterization of the complex [Au(PPh$_3$)(AN3*E*)]PF$_6$ (1). An ethanolic solution (5 mL) of AgNO$_3$ (0.202 mmol), 34.4 mg) was added through a cannula to a solution of [AuCl(PPh$_3$)] (0.202 mmol, 100 mg) in CH$_2$Cl$_2$ (10 mL), causing the immediate precipitation of AgCl. The reaction mixture was kept under constant stirring for 30 min at room temperature in dark and was filtered by means of a cannula to separate the AgCl previously formed. Ligand AN3*E* (0.202 mmol, 62.6 mg) and NH$_4$PF$_6$ (0.202 mmol) were dissolved in a mixture of CH$_2$Cl$_2$/EtOH (15 mL, 2:1, v/v) and were added by cannula to the filtrate afterwards. The solution color changed spontaneously from orange to red and it was stirred for 24 hours, at room temperature and protected from light. Finally, the solution was concentrated under reduced pressure and the addition of hexane portions gave rise to the precipitation of a red solid which was filtered on a porous glass plate and dried *in vacuo*. Yield: 77%. Anal. Calcd for C$_{40}$H$_{30}$NF$_6$OP$_2$Au: C, 52.59; H, 3.31; N, 1.53. Found: C, 52.33; H, 3.39; N, 1.78. Mp: 241 ºC (dec). ^{1}H NMR (400 MHz, CDCl$_3$, TMS): 8.92 (m, 3H, H$_b$ + H$_{A2}$); 8.51 (s, 1H, H$_{B10}$); 8.26 (d, 2H, H$_{B1}$, J$_{H-H}$ = 8 Hz); 8.18 (d, 2H, H$_{A3}$, J$_{H-H}$ = 6 Hz); 8.03 (d, 2H, H$_{B4}$, J$_{H-H}$ = 8 Hz); 7.57 (m, 17H, PPh$_3$ + H$_{B2}$); 7.51 (m, 3H, H$_{B3}$ + H$_a$). ^{31}P NMR (162 MHz, CDCl$_3$, H$_3$PO$_4$): 29.1 (s, 1P, PPh$_3$); -144.19 (sept., J$_{P-F}$ = 713 Hz). ^{13}C NMR (100.8 MHz, CDCl$_3$, TMS): 187.40; 152.19 (C$_{A2}$); 145.55 (C$_b$); 134.20; 132.74 (C$_{PPh3}$); 131.19; 129.83 (C$_{B10}$); 129.71 (C$_{PPh3}$); 129.08 (C$_{B4}$); 128.84 (C$_a$); 128.46; 127.23 (C$_{B2}$); 126.97;

126.3; 125.62 (C_{B3}); 124.78 (C_{B1}); 124.33 (C_{A3}). Positive-ion ESI mass spectra ion cluster (DMSO) at m/z 768.17 [$C_{40}H_{30}NOPAu$]$^+$. $\varepsilon_{258} = 92881$ M^{-1} cm^{-1}; $\varepsilon_{426} = 7720$ M^{-1} cm^{-1} (in DMSO).

Synthesis and characterization of the complex [Au(SIMes)(AN3*E*)]PF$_6$ (2). An ethanolic solution (7 mL) of AgNO$_3$ (0.186 mmol, 31.5 mg) was added via cannula to a Schlenk tube containing 13 mL of a solution of [AuCl(SIMes)] (0.186 mmol, 100 mg) in CH$_2$Cl$_2$, causing the immediate precipitation of AgCl. The reaction mixture was kept under constant stirring for 30 min at room temperature and protected from light. The solution was transferred, by cannula provided with a filter to remove the formed AgCl, to another Schlenk containing ligand AN3*E* (0.186 mmol, 57.4 mg) and NH$_4$PF$_6$ (0.186 mmol, 30.3 mg) in the mixture CH$_2$Cl$_2$/EtOH (21 mL, 2:1, v/v) as solvents. The solution color changed immediately from orange to intense red and it was kept in constant stirring for 24 hours in dark conditions. The solution was concentrated under reduced pressure afterwards and portions of hexane were added until the precipitation of a red solid which was filtered with a porous glass plate and dried *in vacuo*. Yield: 92%. Anal. Calcd for $C_{43}H_{41}N_3F_6OPAu$: C, 53.93; H, 4.31; N, 4.39. Found: C, 53.40; H, 3.98; N, 4.01. Mp: 188 ºC (dec). ^{1}H NMR (400 MHz, CDCl$_3$, TMS): 8.80 (d, 1H, H$_b$, $J_{HH} = 16$ Hz); 8.47 (s, 1H, H$_{B10}$); 8.20 (m, 4H, H$_{A2}$ + H$_{B1}$); 8.00 (m, 4H, H$_{A3}$ + H$_{B4}$); 7.53 (m, 2H, H$_{B2}$); 7.45 (m, 2H, H$_{B3}$); 7.35 (d, 1H, H$_a$, $J_{HH} = 16$ Hz); 7,01 (s, 4H, H$_{C3}$); 4.18 (s, 4H, H$_{D2}$); 2.38 (s, 12H, -CH$_{3a}$); 2.31 (s, 6H, -CH$_{3b}$). ^{31}P NMR (162 MHz, CDCl$_3$, H$_3$PO$_4$): -144.31 (sept., $J_{P-F} = 711$ Hz). ^{13}C NMR (100.8 MHz, CDCl$_3$, TMS): 188.59; 186.24 (C); 151.67 (C_{A2}); 146.89; 145.11 (C_b); 139.12; 135.20; 136.60; 130.72; 129.52 (C_{C3}); 129.39 (C_{B10}); 128.65 (C_{A3}/C_{B4}); 127.76 (C_a); 126.86 (C_{B2}); 125.23 (C_{B3}); 124.30 (C_{B1}/C_{A3}/C_{B4}); 50.83 (C_{D2}); 20.72 (-CH$_{3b}$); 17.61 (-CH$_{3a}$). Positive-ion ESI mass spectra ion cluster (DMSO) at m/z 812.29 [$C_{43}H_{41}N_3OAu$]$^+$. $\varepsilon_{259} = 93240$ M^{-1} cm^{-1}; $\varepsilon_{426} = 6860$ M^{-1} cm^{-1} (in DMSO).
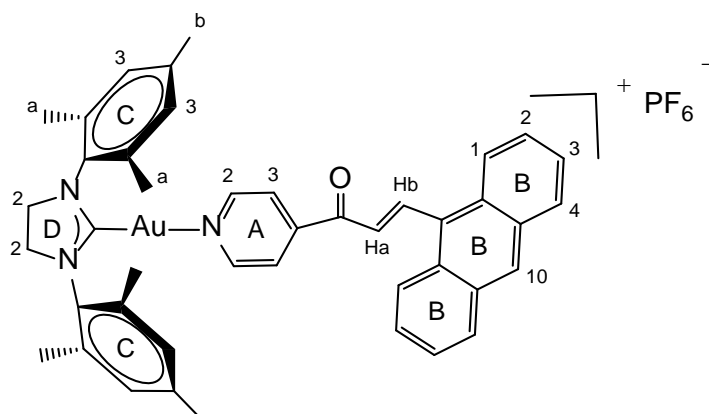

Figure 11. Coding system used for NMR signals assignment of the complex **2**.

X-ray Crystal Structure Analysis. Crystals suitable for X-ray diffraction of ($C_{40}H_{30}AuNOP$)·(PF$_6$)·0.5CH$_2$Cl$_2$ were obtained from dichloromethane/hexane and

16

mounted in inert oil on a glass fiber and transferred to the diffractometer. Details of the X-ray structure determination and refinement parameters for the compound are given in Table S1 [†]. Intensities were registered at 100K on a Bruker D8QUEST diffractometer using monochromated Mo $K\alpha$ radiation (λ = 0.71073Å) in ω and φ scan mode. The structure was solved by dual methods (SHELXT 2014/5);[42] refinement was done by full-matrix least squares on F^2 using the SHELXL-2018/1 program suite;[43] empirical (multi-scan) absorption correction with SADABS -2016/2 (Bruker).[44] Graphics were drawn with OLEX2.[45] Special features of **1:** One phenyl ring is disordered over two positions, ca: 55:45%.

Stability Studies. The stability of the cytotoxic compounds **1** and **2** has been tested in DMSO solution (1 mg/mL) and in a mixture of DMSO/H$_2$O (1:1, v/v, 10^{-3} M) in the presence of an excess of NaCl (100 mM) by ESI mass spectrometry (positive mode), as well as in the pseudophysiological DMSO/DMEM medium (1:1, v/v, 10^{-4} M) by absorption spectroscopy.

Cell lines and culture. HT-29 (ACC-299), HCT-116 (ACC-581), and DLD-1 (ACC-278) colon carcinoma, and MCF-7$^{\text{Topo}}$ (ACC-115) breast cancer cells were cultured in Dulbecco's modified Eagle Medium (DMEM, Biochrom) containing 10% fetal bovine serum (FBS; Biochrom) and 2 mM L-glutamine and 1% penicillin/streptomycin at 37 °C, 5% CO2, and 95% humidified atmosphere. MCF-7$^{\text{Topo}}$ cells were treated with the maximum-tolerated dose of topotecan, respectively 24 h after every cell passage to keep them multi-drug resistant. The cells lines were confirmed to be mycoplasma-free using Hoechst DNA staining method.[46] The maximum % of DMSO used was 0.4 (except for cisplatin, water diluted) and the measurements were corrected with a control containing the same amount of DMSO.

***In vitro* growth inhibition.** Cell viability was determined using a 3-(4,5-dimethylthiazo-2-yl)-2,5-diphenyl-tetrazolium bromide (MTT)-based assay after exposure of the compounds. Cells were cultured in 96-well plates at a density of 5000 cells/well in complete medium and incubated for 24 h. Dilutions of chemical complexes were added at the final concentrations in the range of 0 to 100 μM in a final volume of 111.1 μL per well and incubated for 72 h. The drug-containing medium was replaced by 50 μL of a MTT solution (0.05 % in PBS). After incubation of the cells for 2 h at 37 °C, the MTT solution was removed and 25 μL of a SDS/DMSO solution (10 %) were added to solubilize the purple formazan crystals formed in active mitochondria. The absorbance of MTT was measured at 570 nm, the absorbance of the background at 630 nm using a microplate reader (Tecan F200). The IC$_{50}$ values were calculated based on the inhibitory rate curves using the next the equation:

$$I = \frac{I_{max}}{1 + \left(\frac{IC_{50}}{c}\right)^n}$$

Where *I* represent the percentage inhibition of viability observed, *Imax* is the maximal inhibitory effect, *IC$_{50}$* is the concentration that inhibits 50% of maximal growth, *C* is the

concentration of the compound and n is the slope of the semi-logarithmic dose-response sigmoidal curves. The non-linear fitting was performed using GraphPad Prism. All compounds were tested at least in four independent studies.

Metal accumulation in cancer cells. The HT29 cells were seeded at $5 \cdot 10^5$ cells/well in 6-well plates in 1.8 mL of complete growth medium. After 24 h or incubation, the cells were treated with 2 µM of the tested compounds for additional 24 h. Cells were then trypsinized, counted and the pellets digested using Suprapur® nitric acid 30 %. The amount of metal elements Au and Pt was determined using Inductively Coupled Plasma Mass Spectrometry (ICP-MS).

Mitochondrial polarization assay. Mitochondrial membrane potential was evaluated with the fluorescent probe Rhodamine-123 (Sigma-Aldrich). HT29 cells in the density of 2×10^4 were seeded for 24 h in complete medium on 96-well plates and then treated with the test compounds or carbonyl cyanide m-chlorophenylhydrazone 10 µM for 24 h. Untreated cells were treated with the vehicle DMSO 0.4%. Drug-containing medium was suctioned and a solution of Rhodamine-123 1 µM was added for 20 min at room temperature. Microplates were then scanned on a FLUOstar Omega spectrofluorometer with excitation and emission wavelengths 488 nm and 530 nm, respectively. Experiments were repeated in duplicate using triplicate points per concentration level.

Apoptosis assay. The apoptotic or necrotic induction of the gold complexes on HT29 cells was evaluated using the FITC-Annexin V/Propidium Iodide (PI) labelling method. In brief, HT29 cells were seeded in 12-well plates at a density of $3 \cdot 10^5$ cells/well and incubated overnight. Treatment with 10 µM of gold complexes or cisplatin was added for 24h or 48 h. The cells were then harvested, washed with PBS, centrifuged and the pellets were resuspended in 185 µL binding buffer. Then, 5 µL FITC-Annexin-V and 10 µL PI were added and protected from light for 15 min. Cells were analyzed by flow cytometry (Beckman CoulterEpics XL) and a total of 10 000 events were acquired in each sample, registering at 620 and 525 nm for PI and Annexin V, respectively, λ_{exc} = 488 nm. Data were analyzed using FlowingSoftware version 2.5.1. Experiments were repeated in duplicate yielding similar results (n=2).

Flow cytometric analysis of cell cycle distribution. HT29 cells were seeded into 6-well plates at a density of $3 \cdot 10^5$ cells/well. Treatment with either DMSO alone or with 10 µM of gold compounds or cisplatin was added for 24 h. Then cells were trypsinized, fixed in 70% ice-cold ethanol for 1 h, followed by staining with 40 µg/mLPI for 30 min and analyzed using Beckman CoulterEpics cytometer (λ_{exc} = 488 nm and λ_{em} = 630). Data were analyzed using FL2-A channel with FlowingSoftware version 2.5.1. Experiments were repeated in duplicate (n=2).

ROS induction assay. HT29 cells in the density of $2 \cdot 10^4$ were seeded for 24 h in 200 µL per well complete medium without Phenol Red on 96-well black plates. Cells were then washed with PBS and incubated with 10 µM 2´,7'-dichlorodihydrofluorescein diacetate (DCFH-DA) for 30 min at 310 K. After incubation, DCFH-DA solution was removed, and gold compounds diluted in cell culture medium without phenol red were

added to the cells at appropriate concentrations for 2 hours. Fluorescence of DCF product was measured using FLUOstar Omega spectrofluorometer. Experiments were repeated in triplicate with quadruplicate points.

Reaction with 9-Ethylguanine (9-EtG) followed by ESI-MS. Gold(I) complexes were incubated with 9-EtG in a 1:5 molar ratio in DMSO/H_2O (1:1, v/v) at RT. Mass spectra were recorded in different times (0, 7 and 24 h) to follow the reaction. The concentration of compounds was 1.0 mM.

Hoechst 33258 Displacement Experiments. In the Hoechst 33258 fluorescence displacement experiments, 3 mL of a solution 20 μM ct-DNA and 2 μM Hoechst 33258, in Tris-HCl buffer (pH=7) was titrated with aliquots of a concentrated solution of the complex in DMSO producing solutions with varied mole ratios of ct-DNA/complex (0-1:8). After each addition, the solution was stirred at RT for 5 min before measurement. The emission spectra of the solution were obtained by exciting at 338 nm and measuring the emission spectra from 350−650 nm using 5 nm slits, observing an emission maximum wavelength at 462 nm.

Ethidium bromide saturation assay. A 96 black well plate was prepared with wells containing 100 μL of pure TE buffer (10 mM Tris/HCl, 1 mM EDTA, pH 8.0) for background fluorescence measurement and wells containing 100 μL TE buffer with 1 μg salmon sperm DNA. 11.1 μL of appropriate predilutions of **1**, **2**, AN3*E* or the solvent in ddH_2O were added into the wells to give final concentrations of 0 μM, 5 μM, 10 μM, 25 μM or 50 μM. Each concentration was tested in triplicates. After an incubation period of 2 h at 37 °C 100 μL of a 10 μg/mL ethidium bromide solution in TE buffer was added into each well. The fluorescence of intercalated ethidium bromide was measured at λ_{ex} = 535 nm/λ_{em} = 595 nm after 5 min of incubation at RT in the dark. The measured fluorescence values were corrected by their background fluorescence and the fluorescence of the wells containing the tested compounds was calculated relative to the negative control.

Electrophoretic mobility shift assay. 1.5 μg pBR322 plasmid DNA (Thermo Scientific) were incubated with 0, 5, 10, 25 or 50 μM of the test compounds for 24 h in TE buffer (10 mM Tris/HCl, 1 mM EDTA, pH 8.0) with a final sample volume of 20 μL at 37 °C. The samples were separated via agarose gel electrophoresis (1 %) in TBE buffer (90 mM Tris/HCl, 90 mM boric acid, 2.5 mM EDTA, pH 8.3) at 66 V for 4 . The DNA in the gel was stained with ethidium bromide and the bands were documented via UV transilluminator.

References

(1) Zou, T.; Lum, C. T.; Lok, C.-N.; Zhang, J.-J.; Che, C.-M. Chemical biology of anticancer gold(III) and gold(I) complexes. *Chem. Soc. Rev.* **2015**, *44*, 8786.

(2) Gutiérrez, A.; Marzo, I.; Cativiela, C.; Laguna, A.; Gimeno, M. C. Highly Cytotoxic Bioconjugated Gold(I) Complexes with Cysteine-Containing Dipeptides. *Chem. Eur. J.* **2015**, *21*, 11088.

(3)   Fernández-Moreira, V.; Herrera, R. P.; Gimeno, M. C. Anticancer properties of gold complexes with biologically relevant ligands. *Pure Appl. Chem.* **2019**, *91,* 247–269.

(4)   Zou, T.; Lum, C. T.; Chui, S. S.-Y. Gold(III) Complexes Containing N-Heterocyclic Carbene Ligands: Thiol "Switch-on" Fluorescent Probes and Anti-Cancer Agents. *Angew. Chem. Int. Ed.* **2013**, *52*, 2930–2933.

(5)   Liu, W.; Gust, R. Metal N-heterocyclic carbene complexes as potential antitumor metallodrugs. *Chem. Soc. Rev.* **2013**, *42*, 755–773.

(6)   Casini, A.; Messori, L. Molecular mechanisms and proposed targets for selected anticancer gold compounds. *Curr. Top. Med. Chem.* **2011**, *11*, 2647–2660.

(7)   Cutillas, N.; Yellol, G. S.; de Haro, C.; Vicente, C.; Rodríguez, V.; Ruiz, J. Anticancer cyclometalated complexes of platinum group metals and gold. *Coord. Chem. Rev.* **2013**, *257*, 2784–2797.

(8)   Ott, I. On the medicinal chemistry of gold complexes as anticancer drugs. *Coord. Chem. Rev.* **2009**, *253*, 1670–1681.

(9)   Pérez, S. A.; de Haro, C.; Vicente, C.; Donaire, A.; Zamora, A.; Zajac, J.; Kostrhunova, H.; Brabec, V.; Bautista, D.; Ruiz, J. New acridine thiourea gold(I) anticancer agents: Targeting the nucleus and inhibiting vasculogenic mimicry. *ACS Chem Biol.* **2017**, *12*, 1524–1537.

(10)   Hickey, J. L.; Ruhayel, R. A.; Barnard, P. J.; Baker, M. V.; Berners-Price, S. J.; Filipovska, A. Mitochondria-Targeted Chemotherapeutics: The Rational Design of Gold(I) N-Heterocyclic Carbene Complexes that are Selectively Toxic to Cancer Cells and Target Protein Selenols in Preference to Thiols. *J. Am. Chem. Soc.,* **2008,** *130*, 12570–12571.

(11)   Roder, C.; Thomson, M. J. Auranofin: Repurposing an Old Drug for a Golden New Age. *Drugs in R&D*, **2015**, *15*, 13–20.

(12)   Berners-Price, S. J.; Filipovska, A. Gold compounds as therapeutic agents for human deseases. *Metallomics.* **2011**, *3*, 863–873.

(13)   Mora, M.; Gimeno, M. C.; Visbal, R. Recent advances in gold-NHC complexes with biological properties. *Chem. Soc. Rev.*, **2019**, 48, 447–462.

(14)   Oehninger, L.; Rubbiani, R.; Ott, I. N-Heterocyclic carbene metal complexes in medicinal chemistry. *Dalton Trans.,* **2013**, *42*, 3269–3284.

(15)   Mui, Y. F.; Fernández-Gallardo, J.; Elie, B. T; Gubran, A.; Maluenda, I.; Sanaú, M.; Navarro, O.; Contel, M. Titanocene-Gold Complexes Containing N-Heterocyclic Carbene Ligands Inhibit Growth of Prostate, Renal and Colon Cancers in vitro. *Organometallics*, **2016**, *35*, 1218–1227.

(16)   Muenzner, J. K.; Biersack, B.; Albrecht, A.; Rehm, T.; Lacher, U.; Milius, W.; Casini, A.; Zhang, J.-J.; Ott, I.; Brabec, V.; Stuchlikova, O.; Andronache, I. C.; Kaps, L.; Schuppan, D.; Schobert, R. Ferrocenyl-Coupled N-Heterocyclic

Carbene Complexes of Gold(I): A Successful Approach to Multinuclear Anticancer Drugs. *Chem. Eur. J.,* **2016**, *22*, 18953–18962.

(17)   Bertrand, B.; Casini, A. A golden future in medicinal inorganic chemistry: the promise of anticancer gold organometallic compounds. *Dalton Trans.,* **2014**, *43,* 4209–4219.

(18)   Rubbiani, R.; Can, S.; Kitanovic, I.; Alborzinia, H.; Stefanopoulou, M.; Kokoschka, M.; Mönchgesang, S.; Scheldrick, W. S.; Wölf, S.; Ott, I. Comparative in Vitro Evaluation of N-Heterocyclic Carbene Gold(I) Complexes of the Benzimidazolylidene Type. *J. Med. Chem.* **2011**, *54*, 8646–8657.

(19)   Marzo, T.; Cirri, D.; Gabbiani, C.; Gamberri, T.; Magherini, F.; Pratesi, A.; Guerri, A.; Biver, T.; Binacchi, F.; Stefanini, M.; Arcangeli, A.; Messori, L. Auranofin, Et_3PAuCl and Et_3PAuI are Highly Cytotoxic on Colorectal Cancer Cells: A Chemical and Biological Study. *ACS Med. Chem. Lett.,* **2017**, *8*, 997–1001.

(20)   Reddy, T. S.; Privér, S. H.; Rao, V. V.; Mirzadeh, N.; Bhargava, S. K. Gold(I) and gold(III) phosphine complexes: synthesis, anticancer activities towards 2D and 3D cancer models, and apoptosis inducing properties. *Dalton Trans.,* **2018**, *47*, 15312–15323.

(21)   H. Scheffler, Y. You and I. Ott, Comparative studies on the cytotoxicity, cellular and nuclear uptake of a series of chloro gold(I) phosphine complexes. *Polyhedron*, **2010**, *29*, 66–69.

(22)   Ma, L.; Ma, R.; Wang, Y.; Zhu, X.; Zhang, J.; Chan, H. C.; Chen, X.; Zhang, W.; Chiu, S.K.; Zhu, G. Chalcoplatin, a dual-targeting and p53 activator-containing anticancer platinum(IV) prodrug with unique mode of action. *Chem. Commun.,* **2015**, *51*, 6301–6304.

(23)   Ma, L.; Wang, Na.; Ma, R.; Li, C.; Xu, Z.; Tse, M.-K.; Zhu, G. Monochalcoplatin: An Actively Transported, Quickly Reducible, and Highly Potent PtIV Anticancer Prodrug. *Angew. Chem. Int. Ed.* **2018**, *57,* 9098–9102.

(24)   Dabiri, Y.; Abu el Maaty, M. A.; Chan, H. Y.; Wölker, J.; Ott, I. Wölfl, S.; Cheng, X. p53-Dependent Anti-Proliferative and Pro-Apoptotic Effects of a Gold(I) N-Heterocyclic Carbene (NHC) Complex in Colorectal Cancer Cells. *Front. Oncol.,* **2019**, *9*, 438.

(25)   Ali, M.; Dondaine, L.; Adolle, A.; Sampaio, C.; Chotard, F.; Richard, P.; Denat, F.; Bettaieb, A.; Le Gendre, P.; Laurens, V.; Goze, C.; Paul, C.; Bodio, E. Anticancer Agents: Does a Phosphonium Behave Like a Gold(I) Phosphine Complex? Let a "Smart" Probe Answer! *J. Med. Chem.* **2015**, *58*, 4521−4528.

(26)   Sahu, N. K.; Balbhadra, S. S.; Choudhary, J.; Kohli, D.V. Exploring pharmacological significance of chalcone scaffold: a review. *Curr. Med. Chem.,* **2012**, *19,* 209−25.

(27)   Batovska, D. I.; Todorova, I.T. Trends in Utilization of the Pharmacological Potential of Chalcones. *Curr. Clin. Pharmacol.,* **2010**, *5*, 1−29.

(28)   Gomes, M. N.; Muratov, E. N.; Pereira, M.; Peixoto, J. C.; Rosseto, L. P.; Cravo, P. V. L.; Andrade, C. H.; Neves, B. J. Chalcone Derivatives: Promising Starting Points for Drug Design. *Molecules,* **2017,** *22,* 1210.

(29)   Singh, A.; Gut, J.; Rosenthal, P. J.; Kumar, V. 4-Aminoquinoline-ferrocenyl-chalcone conjugates: Synthesis and anti-plasmodial evaluation. *Eur. J. Med. Chem.* **2017**, *125*, 269−277.

(30)   Fernández-Moreira, V.; Val-Campillo, C.; Ospino, I.; Herrera, R. P; Marzo, I.; Laguna, A.; Gimeno, M. C. Bioactive and luminescent indole and isatin based gold(I) derivatives. *Dalton Trans.,* **2019**, *48,* 3098−3108.

(31)   Vergara, E.; Cerrada, E.; Casini, A.; Zava, O.; Laguna, M.; Dyson, P.J. Antiproliferative activity of gold(I) alkyne complexes containing water-soluble phosphane ligands. *Organometallics*, **2010**, *29*, 2596–2603.

(32)   Ruiz, J.; Vicente, C., de Haro, C.; Bautista, D. A novel ruthenium(II) arene based intercalator with potent anticancer activity. *Dalton Trans.*, **2009**, 5071−5073.

(33)   Rehm, T.; Rothemund, M.; Bär, A.; Dietel, T.; Kempe, R.; Kostrhunova, H.; Brabec, V.; Kasparkova, J.; Schobert, R. N,N-Dialkylbenzimidazol-2-ylidene platinum complexes-effects of alkyl residues and ancillary cis-ligands on their anticancer activity. *Dalton Trans.* **2018**, *47,* 17357.

(34)   Novohradsky, V.; Yellol, J.; Stuchlikova, O.; Santana, M. D.; Kostrhunova, H.; Yellol, G.; Kasparkova, J.; Bautista, D.; Ruiz, J.; Brabec, V. Organoruthenium Complexes with C^N Ligands are Highly Potent Cytotoxic Agents that Act by a New Mechanism of Action. *Chem. Eur. J.* **2017**, *23,* 15294−15299.

(35)   Pracharova, J.; Vigueras, G.; Novohradsky, V.; Cutillas, N.; Janiak, C.; Kostrhunova, H.; Kasparkova, J.; Ruiz, J.; Brabec, V. Exploring the Effect of Polypyridyl Ligands on the Anticancer Activity of Phosphorescent Iridium(III) Complexes: From Proteosynthesis Inhibitors to Photodynamic Therapy Agents. *Chem. Eur. J.* **2018**, *24*, 4607−4619

(36)   Cao, J.-J.; Zheng, Y.; Wu, X.-W.; Tan, C.-P.; Chen, M.-H.; Wu, N.; Ji, L.-N.; Mao, Z.-W. Anticancer Cyclometalated Iridium(III) Complexes with Planar Ligands: Mitochondrial DNA Damage and Metabolism Disturbance. *J. Med. Chem.* **2019**, *62,* 3311-3322.

(37)   Ruiz, J.; Vicente, C.; de Haro, C. and Espinosa, A. Synthesis and Antiproliferative Activity of a C,N-Cycloplatinated(II) Complex with a Potentially Intercalative Anthraquinone Pendant. *Inorg. Chem.* **2011**, 50, 6, 2151−2158

(38)   Zamora, A. ; Pérez, S. A. ; Rothemund, M. ; Rodríguez, V. ; Schobert, R. ; Janiak, C. ; Ruiz, J. Exploring the influence of the aromaticity on the anticancer and antivascular activities of organoplatinum(II) complexes. *Chem. Eur. J,* **2017**, *23,* 5614−5625.

(39) Usón, R.; Laguna, A.; Laguna, M.; Briggs, D. A.; Murray, H. H.; Fackler, J. P., (Tetrahydrothiophene)gold(I) of gold(III) complexes. *Inorg. Synth.,* **1989**, *26,* 85−91.

(40) Harrison, M.; Wang, J.; Lin, I. J. B. Facile Synthesis of Silver(I)−Carbene Complexes. Useful Carbene Transfer Agents, *Organometallics,* **1998,** *17*, 972-975.

(41) Constable, E. C.; Zhang, G.; Housecroft, C. E.; Zampese, J. A. 9-Anthracenyl substituted pyridyl enones revisited: photoisomerism in ligands and silver(I) complexes. *Daltons Transactions*, **2011**, *40*, 12146.

(42) Sheldrick, G. M. SHELXT–Integrated space-group and crystal-structure determination. *Acta Cryst*. **2015**, *A71*, 3–8.

(43) Sheldrick, G. M. Crystal structure refinement with SHELXL. *Acta Cryst*. **2015**, *C71*, 3–8.

(44) Krause, L.; Herbst-Irmer, R.; Sheldrick G.M.; Stalke D. Comparison of silver and molybdenum microfocus X-ray sources for single-crystal structure determination. *J. Appl. Cryst.* **2015**, *48*, 3-10.

(45) Dolomanov, O.V.; Bourhis, L.J.; Gildea, R.J.; Howard, J.A.K.; Puschmann, H. OLEX2: A complete structure solution, refinement and analysis program. *J. Appl. Cryst.,* **2009**, *42,* 339-341.

(46) Chen, T. R. Microscopic demonstration of mycoplasma contamination in cell cultures and cell culture media. *Tissue Cult. Assoc. Man.* **1976,** *1,* 229–232.